NJC

Accepted Manuscript



Cite this: DOI: 10.1039/c0xx00000x

www.rsc.org/xxxxxx

ARTICLE TYPE

# Agglomeration of $Pd^0$ nanoparticles causing different catalytic activities of Suzuki carbonylative cross-coupling reactions catalyzed by $Pd^{II}$ and $Pd^0$ immobilized on dopamine-functionalized magnetite nanoparticles

**Yu Long, Kun Liang, Jianrui Niu, Xin Tong, Bing Yuan, Jiantai Ma***

***Received (in XXX, XXX) Xth XXXXXXXXX 20XX, Accepted Xth XXXXXXXXX 20XX***
**DOI: 10.1039/b000000x**



Solvent-dispersible magnetite nanoparticles ($Fe_3O_4$) end-functionalized with amino groups were successfully prepared by a facile one-pot template-free method to immobilize $Pd^{II}$ and $Pd^0$ with a metal adsorption and reduction procedure. They were characterized by TEM, XRD, XPS, FT-IR and VSM. Interestingly, $Pd^{II}$ catalyst exhibited better catalytic activity for carbonylative cross-coupling reactions than $Pd^0$ catalyst. According to the catalytic activities of a variety of arylboronic acids and aryl iodides catalyzed by two kinds of Pd catalysts, proposed reaction mechanism of Suzuki carbonylative cross-coupling reactions by Pd catalyst were also inferred. More importantly, agglomeration of $Pd^0$ nanoparticles was obviously observed in the TEM images of the catalysts after reactions. Therefore, agglomeration of $Pd^0$ nanoparticles should be considered as a significant reason for different catalytic activities of the reactions catalyzed by immobilized $Pd^{II}$ and $Pd^0$ catalysts. Furthermore, the $Pd^{II}$ catalyst revealed high efficiency and stability during recycling stages.

## Introduction

Synthesis of biaryl and heteroaryl carbonyl compounds has attracted considerable interest, since these compounds are important moieties in many biologically active molecules, natural products, and pharmaceuticals.[1] A variety of methods have been reported for their preparation.[2] Among them, Suzuki carbonylative coupling reaction is one of the most promising routes for the direct synthesis of biaryl ketones from carbon monoxide, as aryl halides and arylboronic acids with various functionalities can be tolerated on either partner and arylboronic acids are generally nontoxic and thermally-, air- and moisture-stable.[3] In recent years, many palladium-based homogeneous catalysts possess many merits, such as high reaction rate, high turnover number and efficient selectivity.[4] However, one of the greatest drawbacks of such catalysis is that the products might be contaminated by metalleaching.[5] Additionally, Pd is not common and cheap enough for widespread applications. So it is a big challenge to avoid Pd leach, improve the efficiency and increase recycle rate. A heterogeneous Pd-catalyst can efficiently solve these problems since heterogeneous system is facile to be handled and recovered. Therefore, supported Pd-catalysts can offer high activity and selectivity in the carbonylative coupling reactions.[6]

In recent years, there has been an increasing trend toward the use of magnetically retrievable materials in a variety of areas.[7] $Fe_3O_4$ as a superior magnetic material, has been used in efficient green chemical synthesis and biomedical sciences.[8] Nevertheless it was difficult to be used directly, so surface modification with active groups was indispensable for further applications. Primary amino groups may serve as functional groups suitably for the immobilization of Pd. Thus, interest in preparation of shell coated magnetic $Fe_3O_4$ particles functionalized with hydroxyl, carboxyl and primary amino groups is increasing dramatically.[9] Unfortunately, conventional synthetic processes of core-shell particles usually require tedious synthetic steps, long reaction time and toxic solvent. Therefore, developing a simple and facile approach to obtain functionalized magnetic materials is desperately needed.

In the past few years, dopamine (DA) had been used for surface modification of unfunctionalized $Fe_3O_4$ nanoparticles in the literature.[10, 5b] Among them, one-pot solvothermal synthesis dopamine-functionalized magnetite nanoparticles are promising as catalyst carrier due to their favorable solvent-dispersibility and facile template-free preparation method.[5b, 10a] DA with amino groups was used as a surfactant as well as an interparticle linker instead of using the traditional surfactants. In this paper, we stabilized $Pd^{II}$ and $Pd^0$ on $Fe_3O_4$/DA with a metal adsorption and reduction procedure due to the covalent bonding between Pd and amine groups on the surface of $Fe_3O_4$/DA act as a robust anchor and avoid Pd leaching. Furthermore, the dopamine improved the dispersibility of the nanoparticles in aromatic solution. The $Pd^{II}$ and $Pd^0$ catalysts were both used to catalyze Suzuki carbonylative coupling reaction under mild conditions. According to the catalytic activities of the two kinds of Pd catalysts, proposed reaction mechanism and influence factors of Suzuki carbonylative cross-coupling reactions by Pd catalyst were also inferred.

## Experimental

View Article Online
DOI: 10.1039/C4NJ02285H


### Characterization

These magnetic materials were characterized inductively coupled plasma (ICP), powder X-ray diffraction (XRD), transmission electron microscopy (TEM), X-ray photoelectron spectroscopy (XPS), fourier transform-infrared (FT-IR) and vibrating sample magnetometry (VSM). XRD measurement was performed on a Rigaku D/max-2400 diffrctometer using Cu-Kα radiation as the X-ray source in the 2θ range of 10–80 °. The size and morphology of the magnetic nanoparticles were observed by a Tecnai G2 F30 transmission electron microscopy and samples were obtained by placing a drop of a colloidal solution onto a copper grid and evaporated in air at room temperature. Magnetic measurement of $Fe_3O_4$, $Fe_3O_4$/DA, $Fe_3O_4$/DA-$Pd^{II}$ and $Fe_3O_4$/DA-$Pd^0$ was investigated with a Quantum Design vibrating sample magnetometer (VSM) at room temperature in an applied magnetic field sweeping from -15 to 15 kOe. FTIR of the MNCs was examined by using a 170SX spectrometer in the range of 400–4000 $cm^{-1}$. XPS was recorded on a PHI-5702 instrument and the C1s line at 284.8 eV was used as the binding energy reference.

### Synthesis of the DA modified magnetic nanoparticles ($Fe_3O_4$/DA)

Typically[5b, 10a], $FeCl_3$ (0.973 g) was dissolved in ethylene glycol (30mL) to form a clear solution, followed by the addition of NaOAc (1.97 g) and DA (56.9 mg). The mixture was stirred vigorously for 30 min and then sealed in a Teflon-lined stainless-steel autoclave (50 mL capacity). Then the autoclave was heated to and maintained at 200 ℃ for 12 h, and allowed to cool to room temperature. The black products were washed several times with ethanol and dried at 50℃ for 24 h.

### Loading of $Pd^{II}$ on DA functionalized magnetic nanoparticles ($Fe_3O_4$/DA-$Pd^{II}$)

200 mg of as-synthesised $Fe_3O_4$/DA nanoparticles were first dispersed in a 100mL ethanol solution under ultrasonication for 0.5 h. The formed black suspension was ultrasonically mixed with a 10 ml $PdCl_2$ (0.01 M) solution for 1 h, and then the mixed solution (0.01 M) was vigorously stirred for 2 h. The products were obtained with the help of a magnet, washed thoroughly with deionized water and ethanol then dried in a vacuum at room temperature overnight. The loading level of Pd in $Fe_3O_4$/DA-$Pd^{II}$ catalyst was measured to be 3.42 % by AAS.

### Loading of $Pd^0$ on DA functionalized magnetic nanoparticles ($Fe_3O_4$/DA-$Pd^0$)

200 mg of as-synthesised $Fe_3O_4$/DA nanoparticles were first dispersed in a 100mL ethanol solution under ultrasonication for 0.5 h. The formed black suspension was ultrasonically mixed with a 10 ml $PdCl_2$ (0.01 M) solution for 1 h, and then an excess 100 ml $NaBH_4$ solution (0.01 M) was slowly dropped into the above mixture with vigorous stirring. After 6 h of reduction, the products were obtained with the help of a magnet, washed thoroughly with deionized water and ethanol then dried in a vacuum at room temperature overnight. The loading level of Pd in $Fe_3O_4$/DA-$Pd^0$ catalyst was measured to be 4.17 % by AAS.

### General procedure for Suzuki carbonylative coupling reactions

A mixture of aryl iodide (0.5 mmol), arylboronic acid (0.6 mmol), $K_2CO_3$ (1.5 mmol), and 2 mol% palladium catalyst in anisole (5 mL) was stirred at 80 ℃ under 1 atm pressure of CO. After the reaction, the mixture was cooled down to room temperature, separated by magnetic decantation, and the resultant residual mixture was diluted with 10 mL of $H_2O$, followed by extraction with ethyl acetate (2×10 mL). The organic fraction was dried with $MgSO_4$, the solvents were evaporated under reduced pressure and the residue was redissolved in 5 mL of ethanol. An aliquot was taken using a syringe and subjected to GC analysis. Yields were calculated against the consumption of the aryl iodides.

## Result and Discussion

### Catalyst preparation and characterization

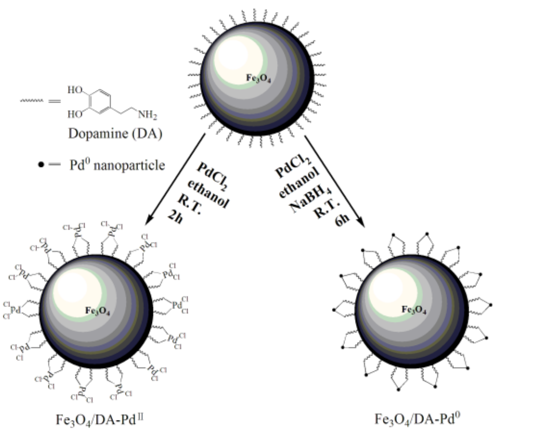


Scheme 1 Preparation of $Fe_3O_4$/DA-$Pd^{II}$ and $Fe_3O_4$/DA-$Pd^0$ catalysts

The process for the preparation of $Fe_3O_4$/DA-$Pd^{II}$ and $Fe_3O_4$/DA-$Pd^0$ catalysts is schematically described in Scheme 1. Briefly, $Fe_3O_4$/DA magnetite nanoparticles were first prepared by a facile one-pot solvothermal synthetic strategy and then immobilized $Pd^{II}$ and $Pd^0$ by the amine groups on the surface of nanoparticles acting as a robust anchor and avoid Pd leaching.

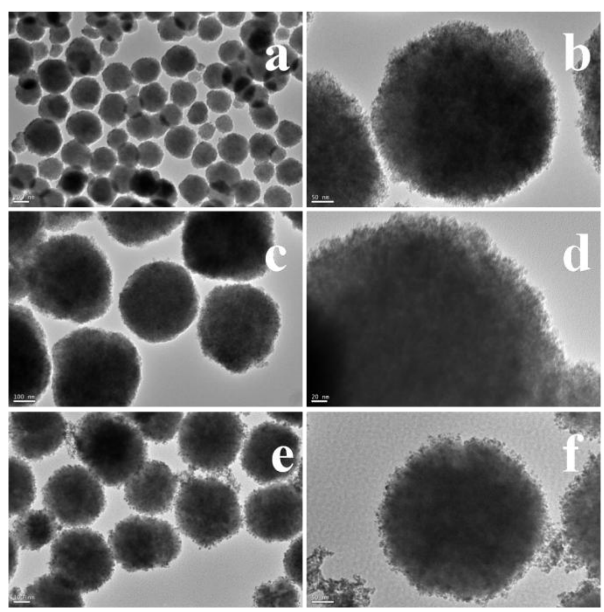


Fig. 1 TEM images of (a, b) $Fe_3O_4$/DA, (c, d) $Fe_3O_4$/DA-$Pd^{II}$ and (e, f) $Fe_3O_4$/DA-$Pd^0$

View Article Online
DOI: 10.1039/C4NJ02285H



Figures 1a and 1b show the typical TEM image of $Fe_3O_4$/DA nanoparticles prepared by the versatile solvothermal reaction. It could be indicated that the $Fe_3O_4$ modified with dopamine was highly dispersed with a spherical shape and a nearly uniform size of approximate 350 nm in diameter. The TEM image exhibited that the $Fe_3O_4$/DA-$Pd^{II}$ (Fig. 1c, d,) and $Fe_3O_4$/DA-$Pd^0$ (Fig. 1e, f), catalyst didn't change considerably after attachment of the palladium onto the surface of the magnetic nanoparticles. From Figure 1c, d, it could be revealed that after fastening $PdCl_2$, no changes of the morphology of these nanoparticles had occurred, and none of Pd or $PdO_x$ nanoparticles were observed in Fig. 1d. As shown in Figure 1e, f, it could also be concluded that the palladium particle size was cantered at about 8 nm. In order to give a powerful evidence of the existence of $Pd^{II}$ and $Pd^0$, EDX spectra of $Fe_3O_4$/DA-$Pd^{II}$ and $Fe_3O_4$/DA-$Pd^0$ was presented in Fig. 2. The peak of copper (Cu) arised from Cu grid in TEM analysis. The peaks corresponding to Pd were expressly found in both EDX spectra of $Fe_3O_4$/DA-$Pd^{II}$ and $Fe_3O_4$/DA-$Pd^0$, and Pd content was 3.35% and 4.26%, respectively, which was almost the same with the content measured by AAS.

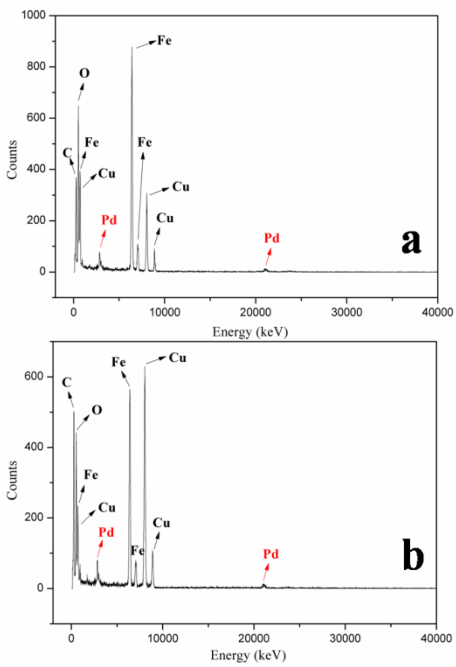


Fig. 2 EDX spectra of (a) $Fe_3O_4$/DA-$Pd^{II}$ and (b) $Fe_3O_4$/DA-$Pd^0$

The crystalline structures of the resulting products were investigated by XRD. In Figure 3, the main peaks of the $Fe_3O_4$/DA-$Pd^{II}$ and $Fe_3O_4$/DA-$Pd^0$ composites were similar to the $Fe_3O_4$/DA. The characteristic diffraction peaks in the samples at 2θ of 30.1°, 35.5°, 43.3°, 53.8°, 57.1° and 62.8° were corresponded to the diffraction of (220), (311), (400), (422), (511) and (440) of the $Fe_3O_4$. All the diffraction peaks matched with the magnetic cubic structure of $Fe_3O_4$ (JCPDS 65-3107)[11] and the sharp and strong peaks confirmed the products were well crystallized. Figure 3c showed that apart from the original peaks, the appearance of the new peaks at 2θ= 39.8, 46.1 and 67.8 were attributed to the $Pd^0$ species, implying that the Pd nanoparticles had been successfully immobilized onto the surface of $Fe_3O_4$/DA.

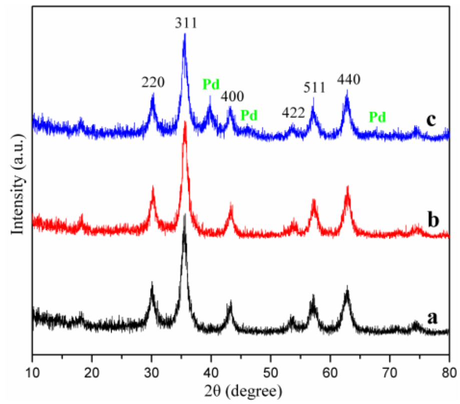


Fig. 3 XRD patterns of (a) $Fe_3O_4$/DA, (b) $Fe_3O_4$/DA-$Pd^{II}$ and (c) $Fe_3O_4$/DA-$Pd^0$

The compositions of $Fe_3O_4$/DA-Pd composite were confirmed by FT-IR (Fig. 4). For comparison, FT-IR of $Fe_3O_4$/DA was also shown in Figure 4a. The bands at 1628, 1473 and 872 $cm^{-1}$ were associated with amine, indicating that plenty of DA molecules were immobilized on the surface of the nanoparticles. The FT-IR spectrum of the $Fe_3O_4$/DA-$Pd^{II}$ and $Fe_3O_4$/DA-$Pd^0$ catalyst (in Fig. 4b, c) demonstrated that almost no change occured after immobilization of palladium on the magnetite nanoparticle surface. Stretching vibrations took place blue shift or red shift, which exhibited $PdCl_2$ and Pd nanoparticles were fastened on the supporter.

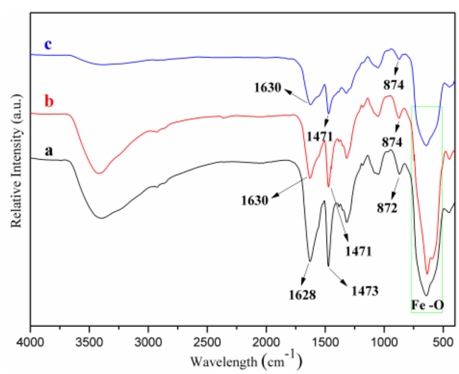


Fig. 4 FT-IR spectra of (a) $Fe_3O_4$/DA, (b) $Fe_3O_4$/DA-$Pd^{II}$ and (c) $Fe_3O_4$/DA-$Pd^0$

Figure 5 presented XPS elemental survey scans of the surface of the $Fe_3O_4$/DA-$Pd^{II}$ and $Fe_3O_4$/DA-$Pd^0$ catalyst. Peaks corresponding to oxygen, carbon, nitrogen, palladium and iron were clearly observed. To establish the oxidation state of Pd in $Fe_3O_4$/DA-$Pd^{II}$ and $Fe_3O_4$/DA-$Pd^0$, XPS analysis was conducted. The Pd $3d_{5/2}$ and Pd $3d_{3/2}$ binding energies of $Fe_3O_4$/DA-$Pd^{II}$ were determined to be 338.8 and 344 eV, respectively (Fig. 5b). These values agreed with the $Pd^{II}$ binding energy of the composite. The binding energy of Pd $3d_{5/2}$ and $3d_{3/2}$ for the $Fe_3O_4$/DA-$Pd^0$ was found to be 334.8 and 340 eV (Fig. 5d), indicating that the loaded Pd nanoparticles were in its 0 state.

View Article Online
DOI: 10.1039/C4NJ02285H



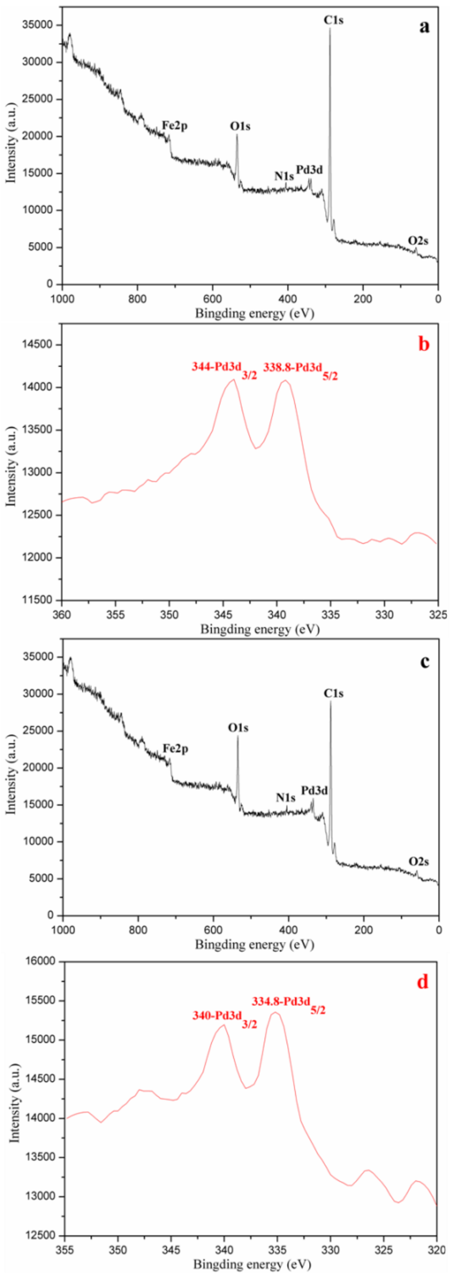


Fig. 5 XPS spectra of (a, b) $Fe_3O_4$/DA-Pd$^{II}$ and (c, d) $Fe_3O_4$/DA-Pd$^0$

The magnetic properties of $Fe_3O_4$/DA, $Fe_3O_4$/DA-Pd$^{II}$ and $Fe_3O_4$/DA-Pd$^0$ were investigated with a VSM at room temperature. As shown in Figure 6, magnetization curves revealed the superparamagnetic behaviour of the magnetic nanoparticles and the magnetic saturations of these were 81.6, 74.1 and 72.5 emu/g, respectively. The decrease of the saturation magnetization suggested the presence of Pd$^{II}$ or Pd$^0$ on the surface of the magnetic support. Even with this reduction in the saturation magnetization, the nanomaterials still could be efficiently separated from the solution with a magnet near the vessels (shown in the insert in Fig. 6).

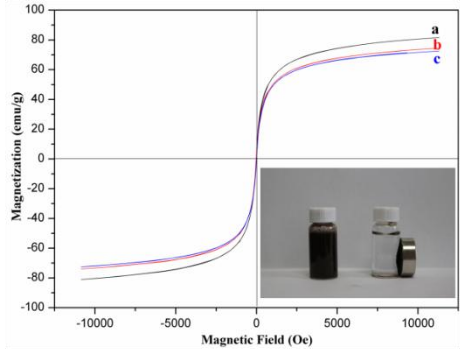


Fig. 6 Room temperature magnetization curves of (a) $Fe_3O_4$/DA, (b) $Fe_3O_4$/DA-Pd$^{II}$ and (c) $Fe_3O_4$/DA-Pd$^0$

**Catalyst testing for the Suzuki carbonylative cross-coupling reactions**

In order to explore the optimal reaction conditions, including temperature, solvent and base, the carbonylative cross-coupling reaction of iodobenzene with phenylboronic acid under an atmospheric pressure of carbon monoxide was chosen as the model reaction. As shown in Table 1, the yields of the target product catalyzed by both $Fe_3O_4$/DA-Pd$^{II}$ and $Fe_3O_4$/DA-Pd$^0$ were low at 40℃ and 60℃ (entry 1-4). When the temperature was increased to 80 ℃, high yields of the target product (93% and 79%) were obtained (Table 1, entry 5, 6). However, the yields of the desired product (91% and 77%) did not increase at 100℃ (Table 1, entry 7, 8). Therefore, 80 ℃ was chosen as the optimum reaction temperature. According to that both less polar solvents (anisole, dioxane and toluene) and polar solvent (DMF) obtained lower yields (Table 1, entry 9-14), non-polar solvent anisole was found to be the best choice of solvent. Under the optimized reaction temperature and solvent, several bases were examined, such as NaOAc, $K_3PO_4$, $Cs_2CO_3$ and $K_2CO_3$ (Table 1, entry 2, 15-20), due to the inorganic bases used in the carbonylative Suzuki coupling reaction could affect the selectivity of the products. As a result, the most used base $K_2CO_3$ was the most efficient base to produce carbonylative coupling product. Therefore, whether using $Fe_3O_4$/DA-Pd$^{II}$ or $Fe_3O_4$/DA-Pd$^0$ as catalyst, the optimized reaction conditions are: 80 ℃, anisole, and $K_2CO_3$. Interestingly, it was obviously revealed that $Fe_3O_4$/DA-Pd$^{II}$ always had a higher yield than $Fe_3O_4$/DA-Pd$^0$ for the carbonylative cross-coupling reaction of iodobenzene with phenylboronic acid under any reaction conditions.

In addition, the prepared $Fe_3O_4$/DA-Pd$^{II}$ and $Fe_3O_4$/DA-Pd$^0$ catalysts revealed similar catalytic activities compared with literature datas on application of the amino-functionalized magnetite nanoparticles supported palladium catalysts as shown in Table 1, entry 21-24. It could be concluded that supported Pd$^{II}$ catalysts exhibited higher catalytic activities for the carbonylative cross-coupling reaction than supported Pd$^0$ catalysts, so were our prepared catalysts.

View Article Online
DOI: 10.1039/C4NJ02285H

Table 1 The carbonylative cross-coupling of iodobenzene with phenylboronic acid under different conditions[a].

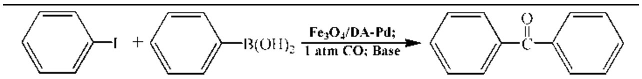


| Entry | Solvent | Base | Catalyst | T/℃ | Yield[b] (%) |
|---|---|---|---|---|---|
| 1 | Anisole | $K_2CO_3$ | $Fe_3O_4$/DA-$Pd^{II}$ | 40 | 9 |
| 2 | Anisole | $K_2CO_3$ | $Fe_3O_4$/DA-$Pd^0$ | 40 | 3 |
| 3 | Anisole | $K_2CO_3$ | $Fe_3O_4$/DA-$Pd^{II}$ | 60 | 46 |
| 4 | Anisole | $K_2CO_3$ | $Fe_3O_4$/DA-$Pd^0$ | 60 | 35 |
| 5 | Anisole | $K_2CO_3$ | $Fe_3O_4$/DA-$Pd^{II}$ | 80 | 93 |
| 6 | Anisole | $K_2CO_3$ | $Fe_3O_4$/DA-$Pd^0$ | 80 | 79 |
| 7 | Anisole | $K_2CO_3$ | $Fe_3O_4$/DA-$Pd^{II}$ | 100 | 91 |
| 8 | Anisole | $K_2CO_3$ | $Fe_3O_4$/DA-$Pd^0$ | 100 | 77 |
| 9 | Toluene | $K_2CO_3$ | $Fe_3O_4$/DA-$Pd^{II}$ | 80 | 51 |
| 10 | Toluene | $K_2CO_3$ | $Fe_3O_4$/DA-$Pd^0$ | 80 | 42 |
| 11 | Dioxane | $K_2CO_3$ | $Fe_3O_4$/DA-$Pd^{II}$ | 80 | 76 |
| 12 | Dioxane | $K_2CO_3$ | $Fe_3O_4$/DA-$Pd^0$ | 80 | 69 |
| 13 | DMF | $K_2CO_3$ | $Fe_3O_4$/DA-$Pd^{II}$ | 80 | 55 |
| 14 | DMF | $K_2CO_3$ | $Fe_3O_4$/DA-$Pd^0$ | 80 | 52 |
| 15 | Anisole | NaOAc | $Fe_3O_4$/DA-$Pd^{II}$ | 80 | <1 |
| 16 | Anisole | NaOAc | $Fe_3O_4$/DA-$Pd^0$ | 80 | <1 |
| 17 | Anisole | $Cs_2CO_3$ | $Fe_3O_4$/DA-$Pd^{II}$ | 80 | 56 |
| 18 | Anisole | $Cs_2CO_3$ | $Fe_3O_4$/DA-$Pd^0$ | 80 | 41 |
| 19 | Anisole | $K_3PO_4$ | $Fe_3O_4$/DA-$Pd^{II}$ | 80 | 59 |
| 20 | Anisole | $K_3PO_4$ | $Fe_3O_4$/DA-$Pd^0$ | 80 | 49 |
| 21 | Anisole | $K_2CO_3$ | $Fe_3O_4$/PPy–$Pd^{II}$ | 80 | 92[c] |
| 22 | Anisole | $K_2CO_3$ | $Fe_3O_4$@$SiO_2$-SH-$Pd^{II}$ | 80 | 91[d] |
| 23 | Anisole | $K_2CO_3$ | $Fe_3O_4$@PNAI-$Pd^{II}$ | 80 | 97[e] |
| 24 | Anisole | $K_2CO_3$ | hollow $Fe_3O_4$-$NH_2$-$Pd^0$ | 90 | 90[f] |

a The reaction was carried out with 0.5 mmol of iodobenzene (0.5 mmol), arylboronic acid (0.6 mmol), CO (1 atm), base (1.5 mmol), solvent (5 mL), 2 mol% palladium catalyst and reaction time: 8h.

b Determined by GC or GC-MS.

c [Ref. 9e] The reaction was carried out with 0.5 mmol of iodobenzene (0.5 mmol), arylboronic acid (0.6 mmol), CO (1 atm), base (1.5 mmol), solvent (5 mL), 2 mol% palladium catalyst and reaction time: 8h.

d [Ref. 3e] The reaction was carried out with 0.5 mmol of iodobenzene (0.5 mmol), arylboronic acid (0.6 mmol), CO (1 atm), base (1.5 mmol), Pd catalyst (1 mol %) in anisole (5 mL) and reaction time: 8h.

e [Ref. 1d] The reaction was carried out with 0.5 mmol of iodobenzene (0.5 mmol), arylboronic acid (0.6 mmol), CO (1 atm), base (1.5 mmol), Pd catalyst (1 mol %) in anisole (5 mL) and reaction time: 8h.

f [Ref. 12] The reaction was carried out with 0.5 mmol of iodobenzene (0.5 mmol), arylboronic acid (0.6 mmol), CO (1 atm), base (1.5 mmol), Pd catalyst (1 mol %) in anisole (5 mL) and reaction time: 12h.

In order to investigate catalytic acivities of $Fe_3O_4$/DA-$Pd^{II}$ and $Fe_3O_4$/DA-$Pd^0$ for carbonylative cross-coupling reaction, a variety of arylboronic acids and aryl iodides was tested under optimized reaction conditions, and the results were shown in Table 2. As expected, $Fe_3O_4$/DA-$Pd^{II}$ always had a higher conversion and target yield than $Fe_3O_4$/DA-$Pd^0$ for the carbonylative cross-coupling reaction of iodobenzene with phenylboronic acid whether using arylboronic acids and aryl iodides containing either electron-withdrawing groups or electron-donating groups (Table 2, entry 1–30). And the carbonylative cross-coupling reactions could proceed smoothly under mild conditions to afford the corresponding carbonylative coupling products in high yields by $Pd^{II}$ catalyst. Furthermore, it was important to receive that aryl iodides substituted with electron-withdrawing groups, such as 4-$CH_3$CO and 2-$NO_2$ (Table 2, entry 7–18), were found to be the most active reagents, since highest TOF was obtained. And since nitryl has stronger electron-withdrawing ability than acetyl, aryl iodides substituted with 4-$CH_3$CO had a higher TOF than aryl iodides substituted (Table 2, entry 7–18), were found to be the most active reagents, since highest TOF was obtained. And since nitryl has stronger electron-withdrawing ability than acetyl, aryl iodides substituted with 4-$CH_3$CO had a higher TOF than aryl iodides substituted with 2-$NO_2$ (Table 2, entry 7–18). In the contrast, aryl iodides substituted with electron-donating groups, such as 4-$CH_3$ and 4-$CH_3$O (Table 2, entry 19–30), exhibited relatively inferior properties. On the other hand, arylboronic acids with different substituents also afforded different yields of target products, especially, had distinct effect for the generation of by-products (Table 2, entry 1–30). It could be concluded that aryl boronic acid containing the electron-attracting group, -Cl, produced the highest yeilds of target products as well as the unacceptable direct coupling products (by-product). Meanwhile, arylboronic acid containing the electron-donating group, –$CH_3$, also showed the lowest yields of target products as well as the unacceptable by-product.

View Article Online
DOI: 10.1039/C4NJ02285H



Table 2 The carbonylative cross-coupling reactions of various aryl iodides with arylboronic acids in the presence of the catalysts[a].

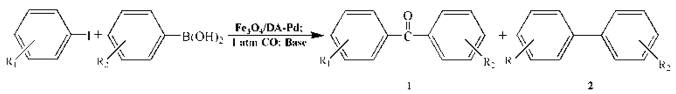


| Entry | $R_1$ | $R_2$ | Catalyst | Time (h) | Yield[b] (%) | | Conversion (%) | TOF[c] ($h^{-1}$) |
|---|---|---|---|---|---|---|---|---|
| | | | | | 1 | 2 | | |
| 1 | H | H | $Pd^{II}$ [d] | 8 | 93 | 5 | 98 | 5.81 |
| 2 | H | H | $Pd^{0}$ [e] | 8 | 79 | 8 | 87 | 4.94 |
| 3 | H | 4-$CH_3$ | $Pd^{II}$ | 8 | 89 | 3 | 92 | 5.56 |
| 4 | H | 4-$CH_3$ | $Pd^{0}$ | 8 | 75 | 7 | 82 | 4.69 |
| 5 | H | 4-Cl | $Pd^{II}$ | 8 | 93 | 6 | 99 | 5.81 |
| 6 | H | 4-Cl | $Pd^{0}$ | 8 | 77 | 11 | 88 | 4.81 |
| 7 | 4-$CH_3$CO | H | $Pd^{II}$ | 6 | 94 | 3 | 97 | 7.83 |
| 8 | 4-$CH_3$CO | H | $Pd^{0}$ | 6 | 80 | 8 | 88 | 6.67 |
| 9 | 4-$CH_3$CO | 4-$CH_3$ | $Pd^{II}$ | 6 | 90 | 3 | 93 | 7.50 |
| 10 | 4-$CH_3$CO | 4-$CH_3$ | $Pd^{0}$ | 6 | 78 | 6 | 84 | 6.50 |
| 11 | 4-$CH_3$CO | 4-Cl | $Pd^{II}$ | 6 | 91 | 4 | 95 | 7.58 |
| 12 | 4-$CH_3$CO | 4-Cl | $Pd^{0}$ | 6 | 79 | 10 | 89 | 6.58 |
| 13 | 2-$NO_2$ | H | $Pd^{II}$ | 6 | 96 | <1 | 97 | 8.0 |
| 14 | 2-$NO_2$ | H | $Pd^{0}$ | 6 | 83 | 7 | 90 | 6.92 |
| 15 | 2-$NO_2$ | 4-$CH_3$ | $Pd^{II}$ | 6 | 92 | <1 | 93 | 7.67 |
| 16 | 2-$NO_2$ | 4-$CH_3$ | $Pd^{0}$ | 6 | 78 | 5 | 83 | 6.50 |
| 17 | 2-$NO_2$ | 4-Cl | $Pd^{II}$ | 6 | 95 | 2 | 97 | 7.92 |
| 18 | 2-$NO_2$ | 4-Cl | $Pd^{0}$ | 6 | 85 | 6 | 91 | 7.08 |
| 19 | 4-$CH_3$ | H | $Pd^{II}$ | 8 | 89 | 3 | 92 | 5.56 |
| 20 | 4-$CH_3$ | H | $Pd^{0}$ | 8 | 74 | 6 | 80 | 4.63 |
| 21 | 4-$CH_3$ | 4-$CH_3$ | $Pd^{II}$ | 8 | 84 | 2 | 86 | 5.25 |
| 22 | 4-$CH_3$ | 4-$CH_3$ | $Pd^{0}$ | 8 | 68 | 5 | 73 | 4.25 |
| 23 | 4-$CH_3$ | 4-Cl | $Pd^{II}$ | 8 | 88 | 6 | 94 | 5.50 |
| 24 | 4-$CH_3$ | 4-Cl | $Pd^{0}$ | 8 | 72 | 10 | 82 | 4.50 |
| 25 | 4-$CH_3$O | H | $Pd^{II}$ | 8 | 86 | 3 | 89 | 5.38 |
| 26 | 4-$CH_3$O | H | $Pd^{0}$ | 8 | 71 | 5 | 76 | 4.44 |
| 27 | 4-$CH_3$O | 4-$CH_3$ | $Pd^{II}$ | 8 | 79 | 2 | 81 | 4.94 |
| 28 | 4-$CH_3$O | 4-$CH_3$ | $Pd^{0}$ | 8 | 62 | 6 | 68 | 3.88 |
| 29 | 4-$CH_3$O | 4-Cl | $Pd^{II}$ | 8 | 87 | 5 | 92 | 5.44 |
| 30 | 4-$CH_3$O | 4-Cl | $Pd^{0}$ | 8 | 65 | 13 | 78 | 4.40 |

a The reactions were carried out with iodobenzene (0.5 mmol), arylboronic acid (0.6 mmol), CO (1 atm), $K_2CO_3$ (1.5 mmol), anisole (5 mL) and 2 mol% palladium catalyst.

b Determined by GC or GC-MS.

c TOF: tmoles of 1-compound yield per mole of Pd per hour.

d $Fe_3O_4$/DA-$Pd^{II}$. e $Fe_3O_4$/DA-$Pd^{0}$.

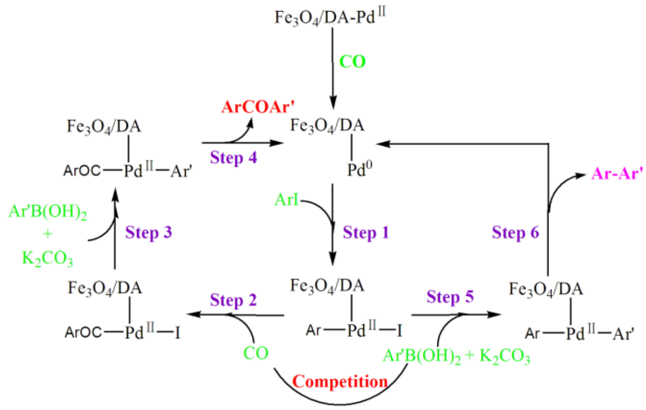


Scheme 2 The proposed reaction mechanisms for catalytic cycles of carbonylative cross-coupling reaction

In order to account for this result, according to the reaction mechanisms proposed in the literature[1d,6c,6e,9e] and combining with the results in Table 2, the proposed reaction mechanism was inferred in Scheme 2. This mechanism scheme was similar with previous, however we came up with a more particular and distinguishing exposition as followed. Firstly, in the step 1, $Pd^0$ was inserted to form $Pd^{II}$ between -ph and -I. Perhaps, the existence of electron-withdrawing groups could reduce electron cloud density of the bond between ph- and I-, resulting in easier formation of bonding pair between phenyl and palladium, thus promoted the oxidative addition of Pd (0). On the contrary, the existence of electron-donating groups went against this step. Hence, aryl iodides substituted with electron-withdrawing groups exhibited higher yields than aryl iodides substituted with electron-donating groups (Table 2, entry 1–30). Secondly, intermediate product was faced with two competition processes, that was step 2 and step 5 as shown in Scheme 2. This competition process was mainly determined by the ability (or rate) of inserting CO and direct coupling with arylboronic acids. Under the same local concentration of CO, arylboronic acids substituted with electron-withdrawing groups were more likely to form direct coupling products, due to the relatively easier connection with phenyl of arylboronic acids caused by electron-withdrawing inductive effect. So, arylboronic acids substituted with electron-withdrawing groups exhibited higher yields of direct coupling products than aryl iodides substituted with electron-donating groups, while the aryl iodides substituted with electron-withdrawing groups was diametrical (Table 2, entry 1–30). Thirdly, in step 3, -I was replaced by the phenyl of arylboronic acids to form carbonylative coupling intermediate product with the aid of $K_2CO_3$. The substituent effect of this step was found to be similar with the step 5. Finally, in step 4 and 6, $Pd^0$ catalyst separated from the complex to form target product and by-product, respectively.

As shown in Scheme 2, catalytic cycles of Suzuki carbonylative cross-coupling reactions were started from the formation of $Pd^0$. Unfortunately, it could be apparently found that $Fe_3O_4$/DA-$Pd^0$ with $Pd^0$ exhibited much more inferior catalytic performance than $Fe_3O_4$/DA-$Pd^{II}$ with $Pd^{II}$ (Table 2, entry 1–30). To our best knowledge, this peculiar catalytic property could be ascribed to that $Pd^0$ nanoparticles are prone to conglomerate in reactions. In order to prove our conjecture, TEM images of $Fe_3O_4$/DA-$Pd^{II}$ and $Fe_3O_4$/DA-$Pd^0$ after Suzuki carbonylative cross-coupling reaction

View Article Online
DOI: 10.1039/C4NJ02285H



were shown in Figure 7 (a, b). Compared with $Pd^0$ nanoparticles of $Fe_3O_4$/DA-$Pd^0$ before the reaction (Fig. 2e, 2f), $Pd^0$ nanoparticles of $Fe_3O_4$/DA-$Pd^0$ after the first cycle of Suzuki carbonylative cross-coupling reaction occurred obvious agglomeration (Fig. 7b). And after 5 cycles of the reaction, the agglomeration of $Pd^0$ nanoparticles became more severe (Fig. 7d). To the contrary, morphology of $Fe_3O_4$/DA-$Pd^{II}$ could be basically considered to maintain invariable after the reactions. It is well known that agglomeration of nanoparticles will significantly reduce the utilization of palladium, thus the relatively inferior catalytic performance of $Fe_3O_4$/DA-$Pd^0$ is acceptant.

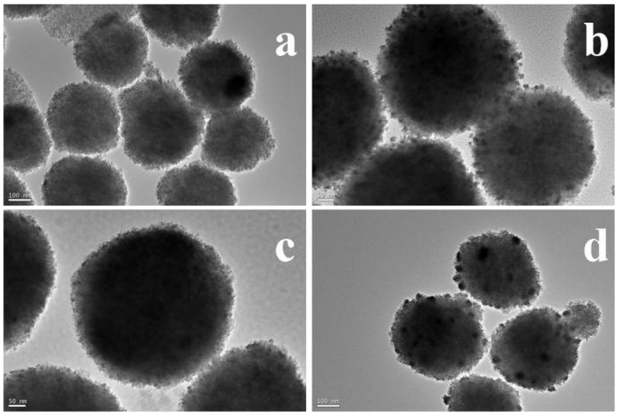

Fig. 7 TEM images of (a) $Fe_3O_4$/DA-$Pd^{II}$ and (b) $Fe_3O_4$/DA-$Pd^0$ after the first cycle of Suzuki carbonylative cross-coupling reaction, (c) $Fe_3O_4$/DA-$Pd^{II}$ and (d) $Fe_3O_4$/DA-$Pd^0$ after 5 cycles of the reaction

As shown in Fig. 7c, some kind of nanoparticles could be observed faintly in the TEM image of $Fe_3O_4$/DA-$Pd^{II}$ after 5 cycles of the reaction, which might be Pd(0) nanoparticles as Pd(Ⅱ) should be reduced to Pd(0) to start the carbonylative cross-coupling reaction. In order to ascertain the state of the palladium in $Fe_3O_4$/DA-$Pd^{II}$ after 5 cycles of the reaction, the recycled catalyst's XPS spectra had been conducted as shown in Fig. 8. It was interesting to observe three peaks assigned to Pd3d with binding energies of 334.8, 339.2 and 344 eV, respectively (Fig. 8b). The XPS result proved the existence of both Pd(Ⅱ) and Pd(0) in the $Fe_3O_4$/DA-$Pd^{II}$ after 5 cycles of the reaction. This could testify the reliability of the proposed reaction mechanism in Scheme 2. On the other hand, since only a part of Pd(Ⅱ) was reduced to Pd(0), the amount of $Pd^0$ nanoparticles in $Fe_3O_4$/DA-$Pd^{II}$ catalyst was much less than $Pd^0$ nanoparticles in $Fe_3O_4$/DA-$Pd^0$, which might be unable to reunite. Therefore, the agglomeration of Pd(0) nanoparticles in $Fe_3O_4$/DA-$Pd^{II}$ catalyst after 5 cycles of the reaction is not obvious.

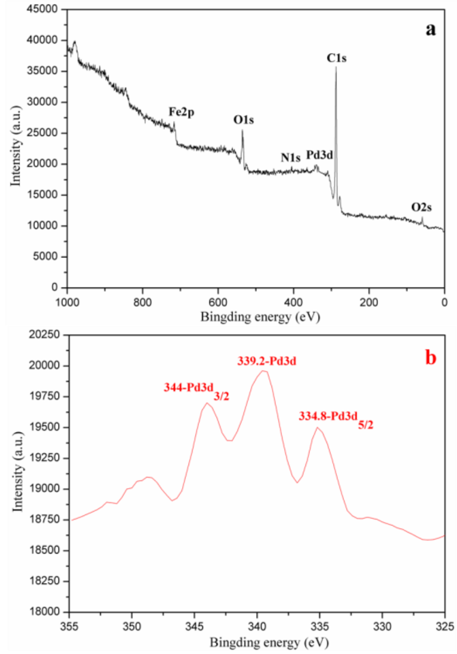

Fig. 8 XPS spectra of $Fe_3O_4$/DA-$Pd^{II}$ after 5 cycles of the reaction

On the other hand, in the catalytic cycles of Suzuki carbonylative cross-coupling reactions catalyzed by $Pd^{II}$ catalyst, $Pd^{II}$ had to be firstly reduced to $Pd^0$ by CO to activate this cycle. In our opinion, this step may be a relatively fast process comparing with steps 1-6, rather than a rate determining step for the catalytic cycle. Importantly, compared with $Pd^0$, the extra process of reducing $Pd^{II}$ certainly led large amount of CO to be absorbed onto the surface of catalyst, resulting in the increase of local concentration of CO. And, high local concentration of CO might be beneficial to obtain target product. Therefore, as shown in Table 2, the TOF and yields of target products catalyzed by $Fe_3O_4$/DA-$Pd^{II}$ were invariably higher than that by $Fe_3O_4$/DA-$Pd^0$ no matter what substrates were tested.

Furthermore, we investigated the recyclability of the $Fe_3O_4$/DA-$Pd^{II}$ and $Fe_3O_4$/DA-$Pd^0$. After the first cycle of the reaction, the catalyst was recovered with the help of a magnet, successively washed with distilled water (to remove excess of base), ethanol, and dried at room temperature ready for the next cycle. The carbonylative cross-coupling reaction of iodobenzene with phenylboronic acid catalyzed by recycled catalyst was displayed in Figure 9. After five times cycles, $Fe_3O_4$/DA-$Pd^{II}$ still maintained high activity with an acceptable decrease. The weight percentage of Pd in $Fe_3O_4$/DA-$Pd^{II}$ and $Fe_3O_4$/DA-$Pd^0$, determined by AAS analysis, was 3.15 % and 3.72 %, affording Pd losses of 7.8% and 10.8%, respectively. Meanwhile, after 5 cycles of the reaction, the agglomeration of $Pd^0$ nanoparticles was very severe (Fig. 7d). It could be concluded that the $Pd^{II}$ of $Fe_3O_4$/DA-$Pd^{II}$ was more stable than the $Pd^0$ of $Fe_3O_4$/DA-$Pd^0$.

View Article Online
DOI: 10.1039/C4NJ02285H


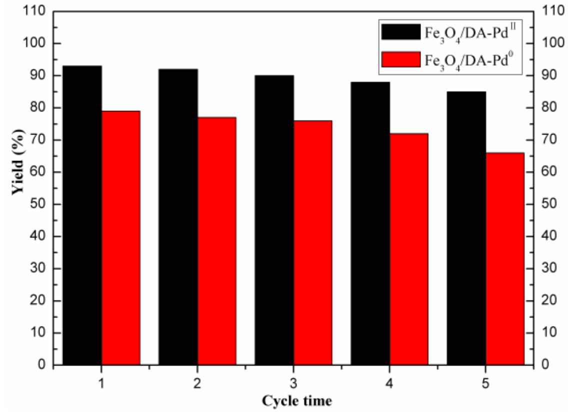


Fig. 9 Recyclability of $Fe_3O_4$/DA-$Pd^{II}$ and $Fe_3O_4$/DA-$Pd^0$ for the Suzuki carbonylative cross-coupling reaction of iodobenzene with phenylboronic acid

## Conclusion

In summary, $Pd^{II}$ and $Pd^0$ were successfully immobilized onto $Fe_3O_4$/DA, which was prepared by a facile one-pot template-free method. The dopamine acted as a robust anchor, avoiding Pd leaching and improving the dispersibility of the nanoparticles in aromatic solution. Contrary to expectation, $Pd^{II}$ catalyst exhibited better catalytic activity for carbonylative cross-coupling reactions than $Pd^0$ catalyst. And substituent group played an important role in the reaction. For instance, both aryl iodides and arylboronic acids substituted with electron-withdrawing groups were beneficial to improve yield of target product, unfortunately, also increase yield of direct coupling product. According to the catalytic activities of a variety of arylboronic acids and aryl iodides catalyzed by the two kinds of Pd catalysts, we came up with a particular and distinguishing exposition about the proposed reaction mechanism of Suzuki carbonylative cross-coupling reactions catalyzed by Pd catalyst. Importantly, agglomeration of $Pd^0$ nanoparticles was obviously observed in the TEM images of the catalysts after the reaction. And after 5 cycles of the reaction, the agglomeration of $Pd^0$ nanoparticles was very severe. Therefore, agglomeration of $Pd^0$ nanoparticles should be considered as a significant reason for different catalytic activities of the reactions catalyzed by immobilized $Pd^{II}$ and $Pd^0$ catalysts. On the other hand, compared with $Pd^0$, the extra process of reducing $Pd^{II}$ to $Pd^0$ certainly led large amount of CO to be absorbed onto the surface of catalyst, resulting in the increase of local concentration of CO. Thus, high local concentration of CO might be beneficial to obtain target product. Furthermore, the $Pd^{II}$ catalyst revealed high efficiency and high stability during recycling stages. We envisaged that our work demonstrated an acceptable reason for the difference of catalytic activities catalyzed by supported $Pd^{II}$ and $Pd^0$. It could enable further implications in a number of other heterogeneous catalytic systems as well.

## Acknowledgements

The authors are grateful to The Fundamental Research Funds for the Central Universities (NO. lzujbky-2014-187), the Key Laboratory of Nonferrous Metals Chemistry and Resources Utilization, Gansu Province for financial support.

## Notes

[a]State Key Laboratory of Applied Organic Chemistry, College of Chemistry and Chemical Engineering, Lanzhou University, Lanzhou, Gansu 730000, P. R. China. Fax: +86-931-891258; Tel: +86-931-8912577; E-mail: majiantai@lzu.edu.cn

## References

1 (a) N. De Kimpe, M. Keppens and G. Froncg, *Chem. Commun.*, 1996, 635; (b) H. L. Li, M. Yang, Y. X. Qi and J. J. Xue, *Eur. J. Org. Chem.*, 2011, 2662; (c) P. J. Tambade, Y. P. Patil, A. G. Panda and B. M. Bhanage, *Eur. J. Org. Chem.*, 2009, 3022; (d) X. Zhu, J. Niu, F. Zhang, J. Zhou, X. Li and J. Ma, *New J. Chem.*, 2014, **38**, 4622.
2 (a) R. K. Dieter, *Tetrahedron*, 1999, **55**, 4177; (b) X. J. Wang, L. Zhang, X. Sun, Y. Xu, D. Krishnamurthy and C. H. Senanayake, *Org. Lett.*, 2005, **7**, 5593; (c) B. Hatano, J. I. Kadokawa and H. Tagaya, *Tetrahedron Lett.*, 2002, **43**, 5859.
3 (a) T. Ishiyama, H. Kizaki, T. Hayashi, A. Suzuki and N.Miyaura, *J. Org. Chem.*, 1998, **63**, 4726; (b) M. V. Khedkar, P. J. Tambade, Z. S. Qureshi and B. M. Bhanage, *Eur. J. Org. Chem.*, 2010, 6981. (c) S. Couve-Bonnaire, J. F. Carpentier, A. Mortreux and Y. Castanet, *Tetrahedron Lett.*, 2001, **42**, 3689; (d) S. Couve-Bonnaire, J. F. Carpentier, A. Mortreux and Y. Castanet, *Tetrahedron*, 2003, **59**, 2793; (e) J.-R. Niu, X. Huo, F.-W. Zhang, H.-B. Wang, P. Zhao, W.-Q. Hu, J. Ma and R. Li, *ChemCatChem*, 2013, **5**, 349.
4 (a) H. L. Li, M. Yang, Y. X. Qi and J. J. Xue, *Eur. J. Org. Chem.*, 2011, 2662; (b) M. Medio-Simon, C. Mollar, N. Rodriguez and G. Asensio, *Org. Lett.*, 2005, **7**, 4669; (c) P. Prediger, A. V. Moro, C. W. Nogueira, L. Savegnaqo, P. H. Menezes, J. B. T. Rocha and G. Zeni, *J. Org. Chem.*, 2006, **71**, 3786; (d) B. M. Okeefe, N. Simmons and S. F. Martin, *Org. Lett.*, 2008, **10**, 5301; (e) M. J. Jacinto, O. H. C. F. Santos, R. F. Jardim, R. Landers and L. M. Rossi, *Appl. Catal. A: Gen.*, 2009, **2**, 117; (f) A. J. Amali and R. K. Rana, *Green Chem.*, 2009, **11**, 1781.
5 (a) M. Cao, Y. Wei, S. Y. Gao and R. Cao, *Catal. Sci. Technol.*, 2012, **2**, 156-163; (b) J. Niu, F. Wang, X. Zhu, J. Zhao and J. Ma, *RSC Adv.*, 2014, **4**, 37761.
6 (a) S. Paul and J. H. Clark, *Green Chem.*, 2003, **5**, 635; (b) H. Q. Yang, X. J. Han, G. Li and Y. W. Wang, *Green Chem.*, 2009, **11**, 1184; (c) M. Z. Cai, G. M. Zheng, L. F. Zha and J. Peng, *Eur. J. Org. Chem.*, 2009, 1585; (d) M. Z. Cai, J. Peng, W. Y. Hao, G. D. Ding, *Green Chem.*, 2011, **13**, 190; (e) M. Z. Cai, G. M. Zheng and G. D. Ding, *Green Chem.*, 2009, **11**, 1687; (f) M. V. Khedkar, P. J. Tambade, Z. S. Qureshi and B. M. Bhanage, *Eur. J. Org. Chem.*, 2010, 6981.
7 (a) J. M. Clemente-Juan, E. Coronado and A. Gaita-Ariño, *Chem. Soc. Rev.*, 2012, **41**, 7464; (b) M. Clemente-León, E. Coronado, C. Martí-Gastaldoz and F. M. Romero, *Chem. Soc. Rev.*, 2011, **40**, 473; (c) E. Coronado and G. M. Espallargas, *Chem. Soc. Rev.*, 2013, **42**, 1525; (d) J. P. Malrieu, R. Caballol, C. J. Calzado, C. Graaf and N. Guihéry, *Chem. Rev.*, 2014, **114**, 429; (e) J. Thévenot, H. Oliveira, O. Sandre and S. Lecommandoux, *Chem. Soc. Rev.*, 2013, **42**, 7099; (f) X-Y. Wang, C. Avendaño and K. R. Dunbar, *Chem. Soc. Rev.*, 2011, **40**, 3213; (g) J. Yuan, Y. Xu and A. H. E. Müller, *Chem. Soc. Rev.*, 2011, **40**, 640.
8 (a) M. A. M. Gijs, F. Lacharme and U. Lehmann, *Chem. Rev.*, 2010, **110**, 1518; (b) J. H. Jung, J. H. Lee and S. Shinkai, *Chem. Soc. Rev.*, 2011, **40**, 4464; (c) S. Laurent, D. Forge, M. Port, A. Roch, C. Robic, L. V. Elst and R. N. Muller, *Chem. Rev.*, 2008, **108**, 2064; (d) A-H. Lu, E. L. Salabas and F. Schüth, *Angew. Chem. Int. Ed.*, 2007, **46**, 1222; (e) Y. Pan, X. Du, F. Zhao and B. Xu, *Chem. Soc. Rev.*, 2012, **41**, 2912; (f) M. B. Gawande, P. S. Branco and R. S. Varma, *Chem. Soc. Rev.*, 2013, **42**, 3371; (g) L. H. Reddy, J. Arias, J. Nicolas and P. Couvreur, *Chem. Rev.*, 2012, **112**, 5818.
9 (a) R. Abu-Reziq, D. Wang, M. Post and H. Alper, *Chem. Mater.*, 2008, **20**, 2544; (b) Y. Q. Wang, B. F. Zou, T. Gao, X. P. Wu, S. Y. Lou and S. M. Zhou, *J. Mater. Chem.*, 2012, **22**, 9034; (c) L. Gai, X. Han, Y. Hou, J. Chen, H. Jiang and X. Chen, *Dalton Trans.*, 2013, **42**, 1820; (d) V. Polshettiwar, R. Luque, A. Fihri, H. Zhu, M. Bouhrara and J. M. Basset, *Chem. Rev.*, 2011, **111**, 3036; (e) J. Niu, M. Xie, X. Zhu, Y. Long, P. Wang, R. Li and J. Ma, *J. Mol. Catal. A: Chem.*,

View Article Online
DOI: 10.1039/C4NJ02285H

2014, **392**, 247; (f) J. Sun, G. Yu, L. Liu, Z. Li, Q. Kan, Q. Huo and J. Guan, *Catal. Sci. Technol.*, 2014, **4**, 1246.

10 (a) H. Zhu, C. Hou, Y. Li, G. Zhao, X. Liu, K. Hou and Y. Li, *Chem. Asian J.*, 2013, **8**, 1447; (b) M. Mazur, A. Barras, V. Kuncser, A. Galatanu, V. Zaitzev, K. V. Turcheniuk, P. Woisel, J. Lyskawa, W. Laure, A. Siriwardena, R. Boukherroub and S. Szunerits, *Nanoscale*, 2013, **5**, 2692; (c) G. Marcelo, A. Muñoz-Bonilla, J. Rodríguez-Hernández and M. Fernández-García, *Polym. Chem.*, 2013, **4**, 558; (d) A. Saha, J. Leazer and R. S. Varma, *Green Chem.*, 2012, **14**, 67; (e) G. Marcelo, A. Muñoz-Bonilla and M. Fernández-García, *J. Phys. Chem. C*, 2012, **116**, 24717; (f) K. H. Bae, Y. B. Kim, Y. Lee, J. Y. Hwang, H. W. Park and T. G. Park, *Bioconjugate Chem.*, 2010, **21**, 505; (g) D. Guin, B. Baruwati and S. V Manorama, *Org. Lett.*, 2007, **9**, 1419.

11 J.-Q. Wan, W. Cai, J.-T. Feng, X.-X. Meng and E.-Z. Liu, *J. Mater. Chem.*, 2007, **17**, 1188.

12 P. Wang, H. Zhu, M. Liu, J. Niu, B. Yuan, R. Li and J. Ma, *RSC Adv.*, 2014, **4**, 28922.